AIAA JOURNAL
Vol. 43, No. 3, March 2005

Planar Particle Imaging Doppler Velocimetry: A Three-Component Velocity Measurement Technique

Mark P. Wernet*
NASA John H. Glenn Research Center at Lewis Field, Cleveland, Ohio 44135

Digital particle imaging velocimetry (DPIV) is a high-resolution, high-accuracy, planar velocimetry technique, which provides valuable instantaneous velocity information in aeropropulsion test facilities. DPIV is capable of providing three-component flowfield measurements using a two-camera, stereo-viewing configuration. Doppler global velocimetry (DGV) is another planar velocimetry technique, which is also capable of providing three-component flow field measurements, but requires three detector systems that must be located at oblique angles from the measurement plane. The three-dimensional configurations of either technique require multiple (DGV) or at least large (stereo PIV) optical access ports in the facility in which the measurements are being conducted. In some test facilities, limited optical access is available (either a single viewing window or small optical access port), which prohibits the implementation of either technique for three-component flow measurements. A hybrid measurement technique is described, called planar particle image Doppler velocimetry (PPIDV), which combines elements from both the DPIV and DGV techniques into a single detection system capable of measuring all three components of velocity across a planar region of a flowfield through a single optical access port. The PPIDV system utilizes common components between the DPIV and DGV systems to reduce system complexity and costs. Measurements of a rotating wheel are used to verify the integrity of the technique. Then simultaneous measurements of a nozzle flow are obtained using both a stereo-viewing DPIV system and a PPIDV system.

Nomenclature

d_o	=	distance from camera lens to object plane
$\boldsymbol{K}$	=	scattering vector, defines measured component of velocity via the Doppler shift
K_i, K_j, K_k	=	i, j, k elements of the scattering vector
$\boldsymbol{k}_i$	=	incident light-sheet propagation vector
$\boldsymbol{k}_o$	=	observation direction
U_j	=	jet efflux velocity
u	=	velocity component along the x axis
u_{LS}, v_{LS}	=	u and v components of velocity in the plane of the light sheet
u', v'	=	u and v components of velocity in the object plane
$\boldsymbol{V}$	=	velocity vector whose elements are (u, v, w)
V_m	=	velocity component measured via the Doppler shifted light
v	=	velocity component along the y axis
w	=	velocity component along the z axis
x_{LS}, y_{LS}	=	x and y displacements in the light-sheet plane
x_0	=	location of velocity measurement in the plane of the light sheet
x', y'	=	x and y coordinates on the object plane
β	=	coupling half-angle in the stereo digital particle imaging velocimetry setup
ΔT	=	interframe time between image exposures
δx	=	particle displacement in the x direction
δz	=	particle displacement in the z direction
θ	=	pan angle of the planar particle image Doppler velocimetry system relative to the plane of the light sheet
λ	=	wavelength of the laser light
ν_D	=	frequency of the Doppler-shifted laser light
ν_0	=	frequency of the laser light
σ_T	=	rss error in the u, v, w velocity measurements
σ_u, σ_v, σ_w	=	standard deviations in the u, v and w velocity measurements

Presented as Paper 2004-0022 at the Aerospace Sciences Meeting, Reno, NV, 5–8 January 2004; received 28 January 2004; accepted for publication 19 May 2004.

*Senior Research Engineer, Optical Instrumentation and NDE Branch, MS-77-1, 21000 Brookpark Road. Associate Fellow AIAA.

Introduction

OPTICAL diagnostic systems play a vital role in the development of new aerospace engines and components. One of the most common and prolific optical diagnostic systems is digital particle imaging velocimetry (DPIV), which is capable of providing two-component measurements of the flow velocity across a planar region of a seeded flowfield. Using a stereo-viewing, dual-camera configuration, DPIV is also capable of providing three-component velocity measurements.[1] Another technique of current interest is Doppler global velocimetry (DGV), also known as planar Doppler velocimetry.[2–4] There are two main implementations of the DGV technique, the first uses a continuous-wave laser in order to obtain time-averaged estimates of the flow velocity,[5] and the second approach uses a pulsed, injection seeded laser to obtain instantaneous flow measurements, similar to those obtained using DPIV.[2] Here we will focus only on the pulsed illumination version of the DGV technique. The main attractions of the DGV technique are that it requires only a single laser pulse to obtain all three components of flow velocity and that it has the potential to yield higher-resolution (single-pixel) estimates of velocity at long imaging distances compared to the somewhat lower resolution obtained with DPIV (nominally 16 pixels between measurements).

The need to acquire all three components of velocity drives the implementation of these three-component velocity measurement techniques. Stereo DPIV is a well-established technique and is widely used. The accuracy in the estimate of the out-of-plane velocity component increases as the coupling angle between the cameras increases. The Scheimpflug condition is typically employed in stereo DPIV systems in order to maintain focus of the particle images across the field of view of the camera.[1] Implementations of the DGV technique require three receiver systems in order to record all three components of the flow. Again the coupling angle between the receiver systems determines the sensitivity of the diagnostic system. One of the difficulties in implementing these two techniques lies in the availability of optical access. Many large-scale wind tunnels and open-jet facilities offer very good optical access. However, some flowfields of interest (compressors, combustion facilities) offer

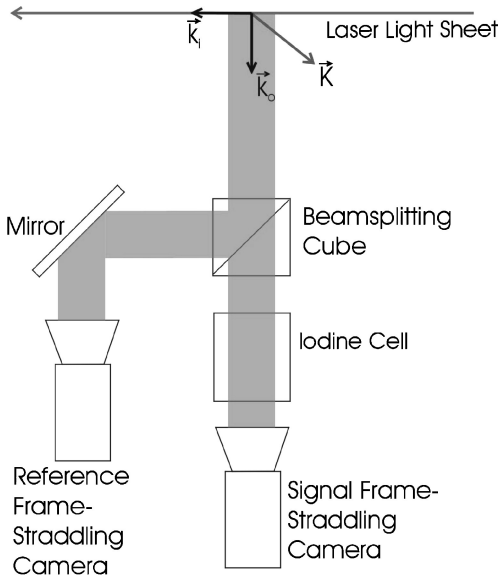

Fig. 1 PPIDV receiver head layout using frame-straddling cameras. The Doppler-shifted light measures the *K* component of velocity.

limited optical access ports. Hence, there is a need for being able to measure all three-velocity components via a single, small optical access port, which is the motivation for this work.

In this paper, a hybrid measurement technique is presented, called planar particle image Doppler velocimetry (PPIDV), which combines elements from both the DPIV and DGV techniques into a single detection system capable of measuring all three components of velocity across a planar region of a flowfield through a single optical access port.[6,7] The main objective of the PPIDV technique is to obtain an out-of-plane velocity estimate without the requirement of a physically separated second receiver system. Two images of the flowfield, closely spaced in time, are required via the DPIV aspect of the technique in order to obtain the in-plane velocity estimates. The out-of-plane velocity estimate is obtained from the Doppler shift of the scattered light. The Doppler shift measurement is obtained via the standard DGV technique, using a signal and reference camera and an iodine vapor cell (Fig. 1). At least one of the laser pulses must be from an injection seeded Nd:YAG laser. The receiver head is constructed similar to that of a standard DGV system, with the exception that "frame-straddling" DPIV type cameras are used. The time between laser pulses is still constrained to provide a valid in-plane velocity measurement. The speckle noise typically found in the DGV technique can be minimized because we only require an out-of-plane velocity measurement at the same resolution as the DPIV measurement. Pixel binning on the order of 16 pixels aids in minimizing the speckle noise. Also, the seeding levels required for the PPIDV technique are the same as those required for DPIV (continuous and uniform).

Background

In the standard DPIV technique, a pulsed laser is used to illuminate the flowfield at two closely spaced instances in time, which are recorded on a frame-straddling charge-coupled-device (CCD) camera, yielding a pair of single-exposure image frames. The DPIV CCD camera is oriented perpendicular to the light sheet, and the processed DPIV data yield the two-component velocity field in the plane of the light sheet.[8]

In the standard DGV technique a single, injection seeded Nd:YAG pulsed laser light sheet illuminates the seeded flowfield, and three receiver systems are used to measure three-components of velocity. The receiver systems are oriented at oblique angles to the light sheet in order to accurately resolve the three-components of velocity.[2] Each DGV receiver system contains two CCD cameras, which share a common view of the illuminated flow through a beam-splitting cube. One camera views the illuminated flow directly (reference camera), and the second camera images the illuminated flow through an iodine cell (signal camera). The laser frequency (wavelength) is adjusted so that the Doppler-shifted light from particles in the flow falls on an iodine absorption feature. The iodine vapor cell acts as a frequency to velocity filter by modulating the intensity of the transmitted light as a function of the flow velocity (Doppler shift). The ratio of the signal and reference images yields the component of the flow velocity along the bisector of the laser-sheet propagation direction and the receiver system observation direction.

The hybrid system employs a single-component DGV receiver system configured to simultaneously acquire DPIV image data, as shown in Fig. 1. The CCD cameras used in the PPIDV receiver head are standard DPIV frame-straddling cameras, yielding two images of the particle-seeded flowfield that are closely spaced in time. The PPIDV system configuration in Fig. 1 shows the receiver system oriented perpendicular to the illuminated plane (as in the standard DPIV configuration). Only one of the laser pulses has to be from an injection-seeded laser to satisfy the requirements of the DGV system; the other laser pulse can be from a standard Nd:YAG laser. The double laser pulse configuration of the illumination system enables the acquisition of DPIV image frame pairs from both the reference and signal cameras. Hence, each camera in the receiver would obtain a pair of image frames. Each image frame pair (signal and reference) is then processed using standard DPIV data-processing techniques to obtain two independent estimates of the two-component in-plane velocity field. The images (from the signal camera and reference cameras) are also processed using standard DGV processing techniques. The configuration of the optical system shown in Fig. 1 enables the DGV system to measure the component of the flow velocity that lies 45 deg out of the plane of the light sheet. The Doppler shift measurement contains contributions from both the u, v, and w components of flow. The DGV velocity measurement is then combined with the in-plane DPIV velocity measurements to extract the full three-component velocity field across the illuminated plane, while viewing through a single optical access port. This is the simplest configuration of the optical system where the DPIV measurements are independent of the w component of velocity.

The component of velocity measured by the Doppler-shifted technique is defined by the scattering vector

$$\boldsymbol{K} = (\boldsymbol{k}_o - \boldsymbol{k}_i) \tag{1}$$

The actual velocity measured via the Doppler shift is given by the dot product of the scattering vector and the three-component velocity vector

$$V_m = \boldsymbol{V} \cdot \boldsymbol{K} = (\nu_D - \nu_0)\lambda = u \cdot K_i + v \cdot K_j + w \cdot K_k \tag{2}$$

u, v, and w are the components of $\boldsymbol{V}$. Equation (2) can be solved for the pure w component of velocity

$$w = (V_m - uK_i - vK_j)/K_k \tag{3}$$

where u and v are assumed to be from the DPIV-measured components of velocity.

The more generalized case of the optical system will now be discussed. In the general case the PPIDV receiver system can view the illuminated plane at an oblique angle. This causes two complications: 1) the DPIV measurements are no longer independent of w, and 2) perspective error is introduced into the DPIV measurements. At this time we are not proposing to enforce the Scheimpflug condition on the optical system. As long as the viewing angle θ is not large, the field of view is not large, and the camera can be operated at a large f/number, then the particle field in the plane of the light sheet remains relatively well focused on the CCD sensor (still a requirement for obtaining DPIV-based velocity estimates).

The tilted optical system measures the particle displacements projected from the plane of the light sheet onto the object plane as shown in Fig. 2. A displacement in the light sheet plane x_{LS} appears as a shorter displacement x'. The mappings for coordinates on the object plane (x', y') onto the plane of the light sheet the are given by[9]

$$x_{\mathrm{LS}} = x'/[\cos\theta - (x'/d_o)\sin\theta] \tag{4}$$

$$y_{\mathrm{LS}} = y'[1 + (x_{\mathrm{LS}}/d_o)\sin\theta] \tag{5}$$

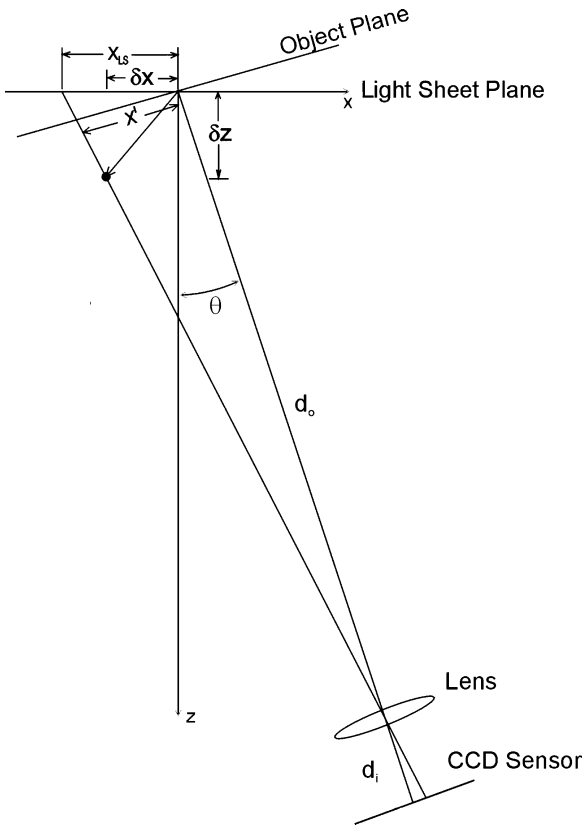

Fig. 2 PPIDV system measures the projected length x_{LS} of the actual particle displacement δx, δz. The pan angle of the receiver system is θ.

where θ is the angle between the optical axis of the receiver head and the normal to the light-sheet plane. The raw images are cross-correlation processed in order to obtain the DPIV estimates of u' and v' in the object plane, which means that the DPIV estimates of velocity are distorted. An alternative approach is to acquire calibration images of a rectilinear target and warp the images before correlation processing, but experience has shown that the distortion of the particle images from the warping process causes a loss of correlation. Instead the distorted images are processed, and the preceding mapping equations are used to correct the correlation-processed DPIV estimates of u' and v' to the correct position and magnitude in the plane of the light sheet u_{LS} and v_{LS}. The mapped velocity v_{LS} is the true v component of velocity measured by the PPIDV system. The mapped u component u_{LS} contains contributions from the w component, which requires further processing steps outlined next.

Figure 2 shows the projected length of a particle displacement having components δx and δz onto the light-sheet plane, resulting in the apparent displacement x_{LS}. The apparent displacement is composed of

$$x_{LS} = \delta x + \delta z\left(\frac{\delta x - d_o \sin\theta + x_0}{d_o \cos\theta - \delta z}\right) \tag{6}$$

The out-of-plane displacement δz manifests itself as an apparent in-plane displacement. Converting the displacements into velocities by dividing through by the time between exposures ΔT, we obtain

$$u_{LS} = u + w\left(\frac{u\Delta T - d_o \sin\theta + x_0}{d_o \cos\theta - w\Delta T}\right) \tag{7}$$

solving Eq. (7) for w:

$$w = \frac{d_o \cos\theta (u_{LS} - u)}{u_{LS}\Delta T - d_o \sin\theta + x_0} \tag{8}$$

which defines w in terms of the displacement-based measurements. Combining this result with Eq. (3) (which defines w in terms of the Doppler shift measurements and displacement-based measurements) and then solving for the true u component of velocity, we find

$$u = \left[\frac{K_k d_o u_{LS}\cos\theta - (V_m - vK_j)(u_{LS}\Delta T - d_o \sin\theta + x_0)}{K_k d_o \cos\theta - K_i u_{LS}\Delta T + K_i d_o \sin\theta - K_i x_0}\right] \tag{9}$$

Hence, by combining the DPIV measurements of u_{LS} and v_{LS} in the plane of the light sheet (of which u_{LS} contaminated by the w component of velocity) with the DGV estimate of V_m, which lies along the vector $\boldsymbol{K}$, we can resolve the true u, v, and w components of velocity across the plane.

DPIV requires imaging the individual particle images, whereas DGV desires multiple particles per pixel on the CCD. DGV is theoretically capable of providing velocity measurements at every pixel in the CCD array (provided there is sufficient particulate seeding in the flow and if the speckle noise can be eliminated; typically 3×3 spatial averaging is required in order to minimize and/or eliminate the laser speckle effect).[10] The image data acquired by the hybrid system must satisfy the DPIV requirement of individually resolved particle images. The hybrid system's DGV-processed images are spatially averaged over subregions corresponding to the size of the spacing between DPIV measurements (nominally 16×16 pixels). Using pixel binning, the Doppler shift estimates are obtained at the same spatial resolution as the DPIV measurements, thereby reducing the need for high seed particle concentrations typically required in the DGV technique. If two injection-seeded lasers are used in the system, then two sets of DGV measurements will be obtained from both the signal and reference cameras and can then be processed to improve the accuracy of the out-of-plane velocity estimate.

Iodine-Cell Calibrations

The iodine cells used in this work were 75-mm-diam, 50-mm-long, vapor limited cells. The iodine-cell vapor pressure is 1.5 torr at 45 C, and the cells were operated at 55 C. The iodine-cell calibrations were obtained by scanning the injection-seeded laser center frequency over the range of 18,789.3–18,790.1 cm^{-1}. The Forkey code was used to generate the expected iodine absorption profiles at the operating conditions of the iodine cell.[11] The scanned intensity ratios were then fit to the Forkey code to determine the operating range of the injection-seeded Nd:YAG laser relative to the iodine-cell's absorption features.

PPIDV Data-Processing Steps

In addition to the receiver head, the PPIDV system uses a laser frequency monitor (LFM) to record each laser pulse. The data-processing steps used in the PPIDV technique are briefly outlined here. First we assume that the signal and reference image frame pairs are cross-correlation processed to obtain the DPIV velocity estimates. Secondly, calibration target images are acquired and processed to determine the grid point center locations. Then the following steps are used:

1) Compute average background image.
2) Compute average frequency flat field (operate laser in broadband mode).
3) Read both PPIDV receiver head and LFM image files.
   a) Subtract background.
   b) Warp the images (bilinear interpolation) using the calibration target coordinates.
      i) This step aligns the images and removes any rotation/magnification differences.
   c) Low-pass filter the images.
   d) Compute LFM image ratio, normalized by frequency flat-field images.
      i) Use I_2 cell calibration to convert ratio to frequency.
      ii) Compute average frequency across the laser beam LFM_AVG.
   e) Compute PPIDV receiver head image ratio, normalized by frequency flat-field images.
      i) Use I_2 cell calibration to convert ratio to frequency.

ii) Subtract LFM_AVG from PPIDV receiver head image frequency to get frequency shift across the imaged field of view.
iii) Multiply frequency shift measurement by λ to obtain V_m.

f) Use Eqs. (4) and (5) to obtain corrected u_{LS} and v_{LS} components of velocity into the plane of the light sheet.
i) This removes the "distortion" in the DPIV measurements caused by the oblique view of the light sheet.

g) Compute the true u component of velocity using V_m via Eq. (9), which removes the out-of-plane motion from the measured in-plane displacement.

h) Compute w component of velocity using V_m and the corrected u and v velocity components via Eq. (3).
i) No correction to v component of velocity is required as long as the PPIDV receiver head is in the same plane as the centerline of the flow being observed (the mapping from v' to v_{LS} provides the only needed correction).

Error Analysis

Absolute Errors

Both the stereo DPIV and PPIDV systems have an inherent systematic measurement error. In stereo DPIV, there is a systematic error in determining the location of the correlation peak, which is nominally accepted to be approximately 0.1 pixels. This absolute error in estimating velocity is scaled by the optical system magnification and the interframe time of the measurement. The error in the in-plane u and v velocity estimates are also functions of the location within the object plane because the perspective distortion introduces some additional error in the measurement. For a stereo DPIV system, the out-of-plane error is related to the in-plane error in the u component of velocity divided by the tangent of the coupling half-angle β (Ref. 1).

In the PPIDV technique the error sources are split between those endemic to the DPIV estimates of the u and v components of velocity and the error sources associated with the Doppler shift measurements of the w component of velocity. The determination of the error in the Doppler shift measurements can be approached in two different ways: 1) theoretical development of all of the contributing error sources in the measurement or 2) measurement of a known flow/object and comparison with the resulting measurements. The theoretical noise contributions developed and applied by McKenzie[12] still resulted in error estimates that did not agree with the experimentally measured errors. Based on these discrepancies, here we will just use the errors determined from measurements of a rotating wheel to define the systematic error in the Doppler shift measurements. The Doppler shift error is fixed and is not affected by the laser pulse interframe time.

The errors in the stereo DPIV technique have been previously analyzed and reported.[1] In the PPIDV technique, the u-component measurements are corrected by the Doppler shift velocity estimates, and then the w component is computed from the corrected u component and the Doppler shift velocity estimate. Because of this interdependence, we need to examine the error in the u, v, and w components of velocity as a function the optical system pan angle. The geometry assumed is that the light sheet lies in the x–y plane and that the w component of velocity lies in the z direction. The PPIDV system has a perpendicular view of the light sheet at $\theta = 0$ deg. The error analysis was performed by numerically differentiating Eqs. (3) and (9) and summing the errors according to[13]

$$\sigma_u^2 = \sum_i \sigma_i^2 \left(\frac{\partial u}{\partial x_i} \right)^2 \tag{10}$$

where we have assumed that the errors are uncorrelated. The errors in estimating the correlation peak location were assumed to be ± 0.1 pixels for the displacement-based estimates, and an error level of 1.6 m/s was assumed for the Doppler shift measurements. (This error level was determined from rotating wheel measurements to be discussed later.) For this analysis, a flowfield with $u = v = 20$ m/s and $w = 240$ m/s was assumed (similar flow properties to the nozzle flow to be studied later). An interframe time of 2.47 μs is selected because of the large w component of velocity and the need to record the same group of particles at both instances that the light sheet is pulsed. The results of this analysis are plotted in Fig. 3. The measurement error in the u, v, and w components are presented in units of meters per second and plotted as a function of pan angle. The evaluations are performed at the center of the field of view of the optical system, at (x, y, z) coordinate of (0,0,0). The perspective distortion in the images caused by the oblique viewing has an additional error contribution (not shown here) to the measurements at points away from the center of the field of view and for increasing pan angle. The error in the v component of velocity is independent of the pan angle, analogous to a stereo DPIV system. At 0-deg pan angle, the u and v displacement-based velocity estimates are independent of the Doppler shift measurements, and for all other angles they are coupled. We see from Fig. 3 that the error in all three velocity components is lowest at a 15-deg pan angle. As the pan angle increases further, the error in w rises sharply. The error in the w component increases as the pan angle increases because for the experimental configuration shown in Fig. 1 the scattering vector $\boldsymbol{K}$ increasingly points away from the z direction and more toward the x direction (V_m is getting smaller). The error in the u component decreases as the pan angle increases as a result of the decreasing magnitude of V_m and the increasing magnitude of the projected in-plane displacement x_{LS}. At large pan angles, u is being estimated from a large value of x_{LS} and a decreasing contribution from V_m, as described by Eq. (9).

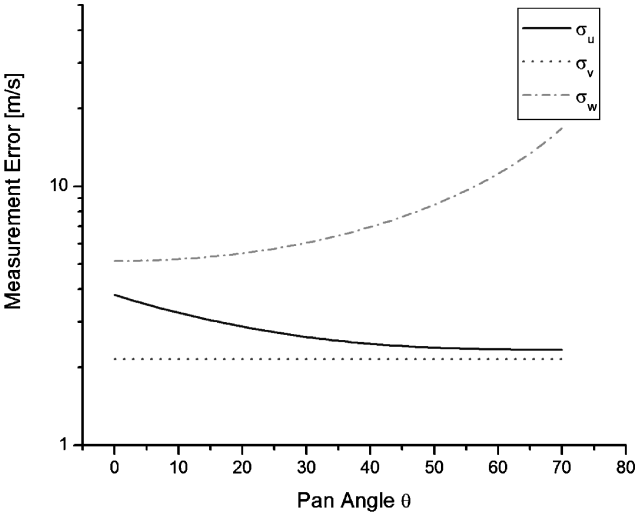

Fig. 3 Errors in the u, v, and w components of velocity are plotted as a function of the pan angle θ for the PPIDV system. The systematic error in the Doppler shift measurement is 1.6 m/s, and based on an interframe time of 2.47 μs, the in-plane systematic error in velocity is 2 m/s.

In general, the absolute errors in u and v for a PPIDV system are comparable to those obtained in a stereo DPIV system. The PPIDV system records two independent records of the particle field, via the signal and reference cameras, which are processed to obtain two independent velocity vector maps. Averaging the two independent measurements together results in a $\sqrt{2}$ reduction in the displacement errors. The accuracy of the v component is essentially the same in the two techniques. The u-component estimate is derived from both the Doppler shift and x-component displacement-based measurements. Because of the Doppler shift contribution and geometric factors, the u-component error is generally larger for PPIDV than for stereo PIV. Similarly, the w-component measurement error can be slightly higher for PPIDV than for stereo DPIV (depending on the experimental configuration). In stereo DPIV, the w-component error starts out large for small coupling angles and decreases rapidly as the coupling angle increases, eventually equaling the in-plane u-component error at a coupling angle of 45 deg. In PPIDV, the w-component error is at a minimum at a pan angle of 0 deg and steadily increases as the pan angle increases. Particular attention to

these properties is critical for the optimal application of the PPIDV technique.

Relative Errors

When using either stereo DPIV or PPIDV to measure flows with a large velocity component out of the light-sheet plane, the apparent in-plane x displacement increases as the coupling angle or pan angle increases, as described by Eq. (6). For the stereo DPIV system, the apparent in-plane motion caused by the out-of plane flow improves the relative accuracy of the u-velocity estimates for increasing coupling half-angle. The w-component error estimates start out very high (100%), but decrease rapidly with increasing coupling angle. The v-component estimates are independent of coupling angle. For the PPIDV system, the u and v error estimates start out approximately the same at 0-deg pan angle. The u-component relative error decreases as a result of the apparent in-plane displacement caused by the large w component. The PPIDV w-component relative error is very low ($\sim$2.2%) as a result of the large out-of-plane velocity.

Experimental Setup

Two different experimental setups were used in this study. In the first setup a rotating wheel was used to determine the minimum resolvable velocity in the PPIDV system. In the second setup, both a stereo DPIV system and the PPIDV system were used to measure the flowfield from a convergent nozzle flow.

Rotating Wheel

A 304-mm-diam, rotating wheel covered with 1200-grit sandpaper was used to provide a simulated flowfield for the PPIDV system. The wheel is equipped with a feedback controller to maintain the rotational speed to ± 1 rpm at 5000 rpm. The wheel was operated at 3000 rpm, providing a tip speed of 47 m/s. The PPIDV rotating wheel measurement setup is shown in Fig. 4. The PPIDV receiver head was oriented perpendicular to the plane of the rotating wheel. The laser illumination was incident on the wheel at 70 deg from the normal to the wheel surface. The wheel was illuminated by passing the laser beam through a ground glass diffuser, which both expanded the laser beam to cover the surface of the wheel and provided relatively uniform illumination across the face of the wheel.

For the experimental configuration shown here, the PPIDV system was used to measure the u component of the wheel velocity, via the Doppler-shifted light. The ensemble average of 54 rotating wheel velocity maps is shown in Figs. 5 and 6. The wheel did not fit completely in the camera field of view for these measurements as evidenced by the clipping of the wheel at the top and bottom. Figure 5 shows a color contour map of the u component of velocity across the face of the wheel. Figure 6 shows a linear, vertical slice through the same velocity map. The data were processed using 16×16 binning, corresponding to the resolution of the velocity vector maps to be obtained when DPIV velocity estimates are extracted from the PPIDV measurements. The linear slice through the middle of the wheel was then fit to a line (where the slope of the line was fixed at the true wheel speed velocity gradient), yielding a standard deviation in the measurements of 1.6 m/s. Hence, we have demonstrated that using our setup we can achieve a minimum absolute velocity error of 1.6 m/s using the Doppler shift measurement.

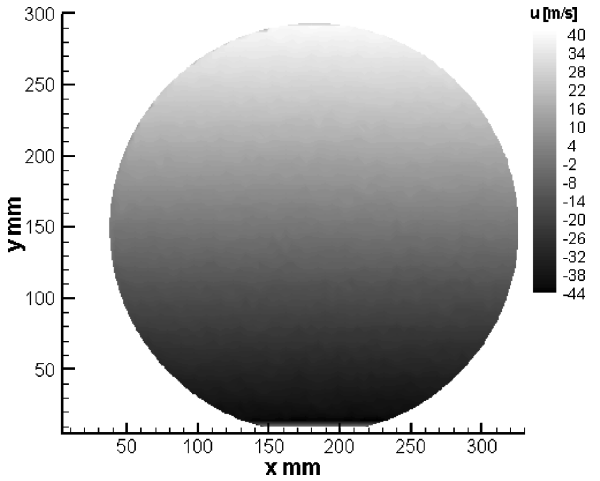

Fig. 5 Measured u component of velocity across the face of the rotating wheel.

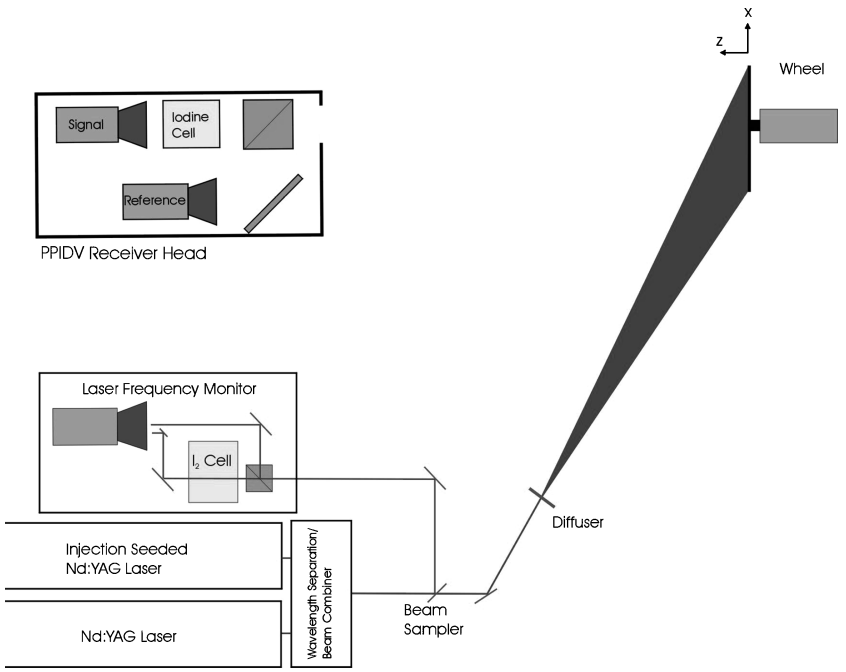

Fig. 4 PPIDV system layout for measurements of a rotating wheel. A diffuser is used to expand the laser beam to illuminate the wheel. The LFM is used to record each laser pulse through a second iodine vapor cell.

Nozzle Flow

To assess the performance of the new PPIDV technique, a direct comparison with an established technique would prove invaluable. Stereo DPIV is an accepted technique and provides a benchmark for comparison of the PPIDV measurement results. An experimental setup was configured as shown in Fig. 7, where we assembled both a stereo DPIV system and the PPIDV system to simultaneously observe a nozzle flow.

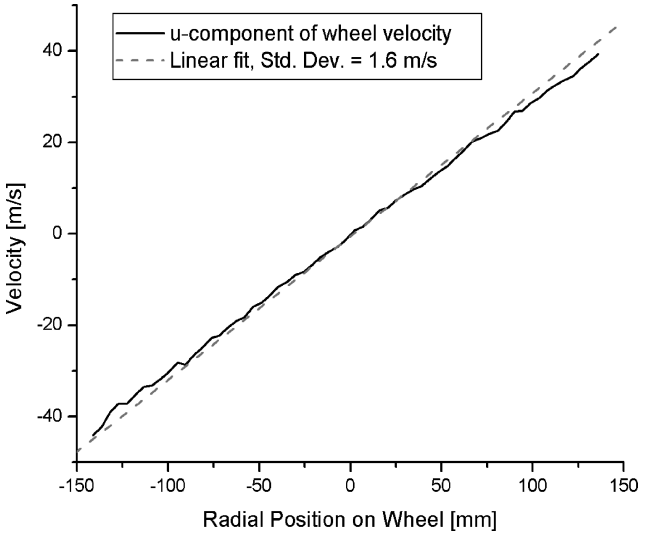

Fig. 6 Vertical slice through the velocity map shown in Fig. 5. A linear fit of the data yields a standard deviation estimate of 1.6 m/s.

The PPIDV receiver head was constructed using two PCO SensiCam cameras for the signal and reference images. The PCO cameras are Peltier cooled and yield 12 bits per pixel at a resolution of 1280×1024 pixels. The PCO cameras are also capable of operating in frame-straddling mode, which is the mode used to acquire short interframe time images for DPIV. A 75-mm, nonpolarizing cube beamsplitter was used to separate the signal and reference image paths inside the receiver head. The cameras were equipped with 105-mm focal length lenses. The 75-mm-diam vapor-limited iodine cells were used to provide the frequency to intensity mapping. The PPIDV receiver head was mounted 16 deg from the nozzle axis, and the PPIDV system field of view was approximately 75×100 mm. For an optical system with the light sheet traveling as shown in Fig. 7, the receiver sensitivity to the w component of velocity is nominally 1.8 MHz/m/s.

A third PCO camera was used in a split image configuration to provide an online, shot-to-shot monitoring of the laser beam spatial frequency distribution (Fig. 7). The LFM also used a vapor-limited iodine cell, operating at 55 C. All three cameras were controlled from a single computer system. The host computer system also contained a National Instruments NI-6602 counter/timer board to provide all of the requisite camera trigger pulses and laser flashlamp and Q-switch pulses. A second National Instruments A/D board was used in the host computer to monitor the iodine-cell temperatures, the laser injection-seed voltage, and the laser Q-switch buildup reduction time voltage. The entire PPIDV acquisition system was controlled by a C++ program.

The pulsed illumination was provided by using two Nd:YAG lasers at 532 nm. Laser A was a Continuum PowerLite 7000 injection seeded laser. Laser B was a Continuum Surelite I. A wavelength separation, beam combining module was used to obtain coaxial beams from the dual laser configuration. Only laser A could be used for

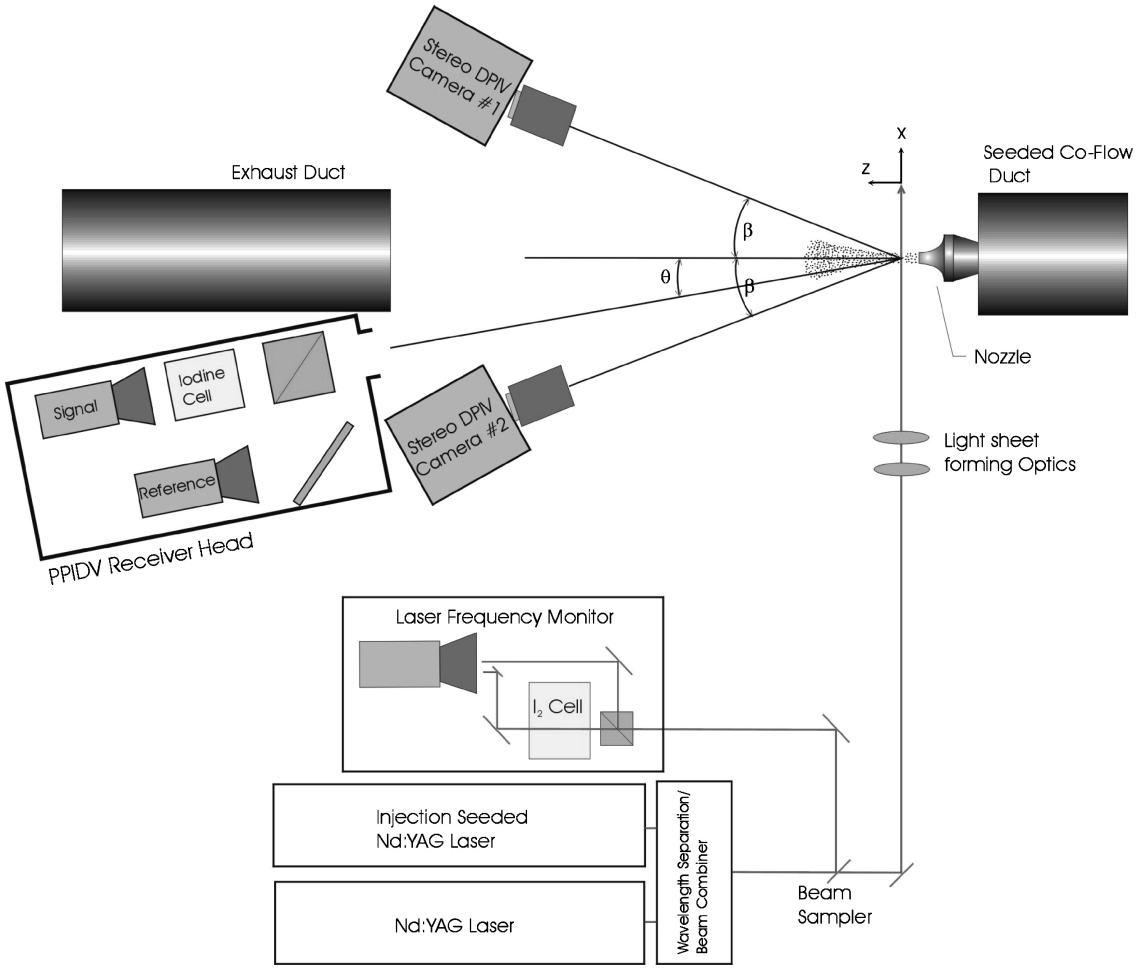

Fig. 7 Layout of PPIDV system and stereo PIV system for simultaneous measurement of nozzle flow. The PIV coupling half angle $\beta = 30$ deg. The PPIDV system pan angle $\theta = 16$ deg. The DPIV system, PPIDV system, and nozzle are all in the same plane.

the Doppler shift measurements. Two laser pulses were required in order to obtain the in-plane DPIV velocity estimates. Future implementations of the PPIDV system can incorporate injection-seeded lasers for both laser pulses, thereby yielding two Doppler shift velocity estimates for each velocity realization. The injected seeded laser frequency was tuned to the desired iodine absorption feature by shifting the seed laser frequency. The seed laser crystal temperature is controlled via a user supplied voltage source. A precision voltage source connected to the seed laser crystal heating circuit was used to control the laser tuning set point and was also used to obtain the iodine-cell calibrations.

The nominal framing rate of the PPIDV system was 3.33 Hz, with the cameras operating in frame-straddle mode (which means image frame pairs were acquired at 3.33 Hz). The laser design operating repetition rate is 10 Hz. To obtain single exposure images on the frame-straddling image pairs, the laser flashlamps were operated at 10 Hz, but the laser Q switches were only fired at the 3.33-Hz rate. This operating mode kept the laser at the nominal thermal operating point, but the low Q-switch firing rate was not sufficient for the laser injection seed locking circuit (which controls the resonator cavity length via the rear cavity mirror mounted on a piezoelectric element) to remain reliably locked. The Q-switch buildup reduction times for each laser pulse were used to determine whether the laser was locked. Data acquired with the laser out of lock were not used in the processing. The laser remained locked about 70% of the time. Future modifications to the system include the incorporation of an external mechanical shutter in the injection-seeded laser beam path, so that the laser flashlamps and Q switches can be operated at 10 Hz, while only illuminating the flowfield at 3.33 Hz.

The stereo DPIV system consisted of two $1k \times 1k$ pixel cameras with a coupling half-angle of ± 30 deg. The cameras were equipped with 60-mm-focal-length lenses, yielding approximately a 50×50 mm field of view. The cameras and lenses were mounted using the Scheimpflug condition. The DPIV system was controlled using the TSI Insight software package. Calibration images of a regular grid target were obtained at five z-axis planes, covering the thickness of the light sheet. A single calibration image for the PPIDV system was obtained at the $z = 0$ plane using the DPIV calibration target.

As mentioned in the beginning of this section, it is highly desirable to have a reference measurement when evaluating a new technique. The PPIDV system was used to control the PCO cameras and the Nd:YAG lasers. A unique aspect of the experiment is that the DPIV cameras were synchronized with the PPIDV cameras, so that the DPIV measurements were obtained using exactly the same laser pulses as were used to record the PPIDV image data. Hence, for each PPIDV instantaneous velocity estimate, we will have a simultaneous three-dimensional PIV velocity estimate for comparison.

The laser light sheet was formed 41 mm from the nozzle exit plane and was oriented perpendicular to the jet axis. The expanded sheet was approximately 2 mm thick and 150 mm wide at the nozzle centerline. The nozzle used to provide the flowfield was a convergent type with an exit diameter of $D = 9.5$ mm. The flow was seeded using a TSI six-jet atomizer filled with Rosco's Smoke Juice. The nominal particle size generated using the seeder was 0.7 μm. The ambient air surrounding the nozzle was seeded by a second six-jet atomizer. A small fan and a 200-mm-diam metal duct were used to provide a low-velocity seeded coflow around the nozzle flow.

Results and Discussion

The convergent nozzle was operated using shop air at a pressure ratio of 0.7, which corresponds to a Mach 0.73 flow (250 m/s) at the nozzle exit. The laser light sheet was positioned 4.3 nozzle diameters downstream from the nozzle exit. The stereo DPIV and PPIDV systems simultaneously acquired image data with an interframe time of 2.47 μs between exposures. A sample image is shown in Fig. 8, where the ambient seeding is observed to be uniform everywhere except the lower right quadrant. Using a single seed injection point in the annular duct surrounding the jet did not supply completely homogenous ambient flow seeding. However, this region of low seed concentration will enable the evaluation of the performance of both techniques under these conditions. The lower right

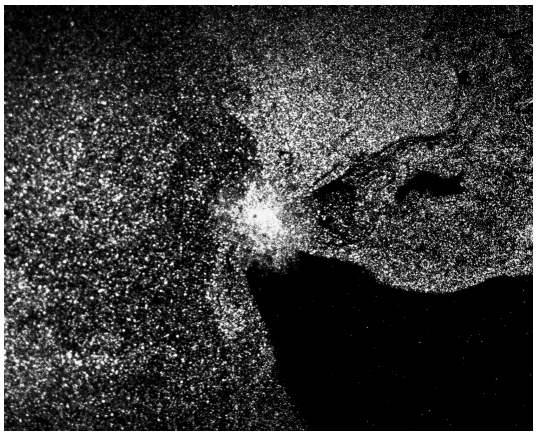

Fig. 8 Sample image of the nozzle flow from the PPIDV system. Note the lack of seed in the lower right region of the image.

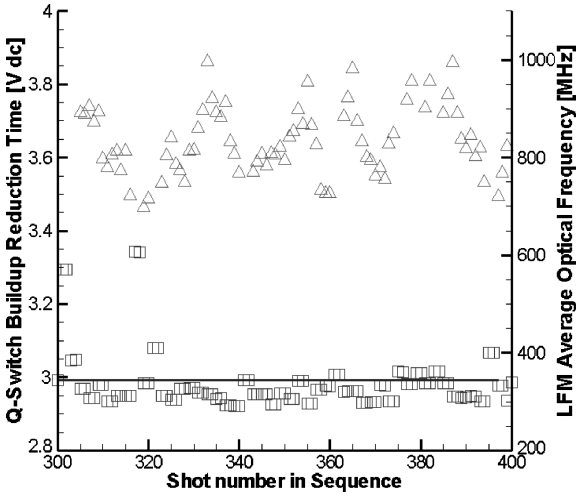

Fig. 9 Q-switch BRT (□) and LFM average optical frequency (△) across the laser beam for a sequence of 100 shots. Q-switch BRTs larger than 2.99 V (those above the horizontal line) are rejected.

portion of the field of view was typically deficient in flow seeding. The nozzle core flow was always well seeded, and good results were obtained in the core flow. A sequence of 100 image pairs was collected for both diagnostic systems. Of the 100 frame pairs, the laser remained locked for 79 shots. The average laser frequency for each shot along with the Q-switch buildup reduction time (BRT) are shown in Fig. 9. The horizontal line in the figure represents the cutoff value used to reject Q-switch BRTs greater than 2.99 V. The mean frequency in the laser beam is observed to vary in an oscillatory manner about a value of 860 MHz. The slow, sinuous variation in laser frequency is caused by operating the laser Q switch at only 3.33 Hz, which impedes the ability of the resonator cavity mirror/piezocircuit to stably lock onto a single frequency. The variation in the average frequency across the laser beam does not affect the measurement accuracy of the technique because the actual velocity measurement is referenced to the average laser frequency, on a shot to shot basis.

The stereo DPIV data were collected and processed using a multipass correlation, where the final grid resolution was 32×32 pixel subregions on 16 pixel centers. The two-dimensional velocity vector maps from the left and right stereo views were then used to compute the three-dimensional vector field. The three-vector maps were then ensemble averaged, using only the data sets that passed the Q-switch BRT test. Hard velocity cutoff limits were used along with Chauvenet's criteria for removing statistical outliers in the ensemble-averaging process.[14] The final three-dimensional velocity vector grid resolution was 1.2 mm between measurements, which was selected to match the spatial resolution of the PPIDV results.

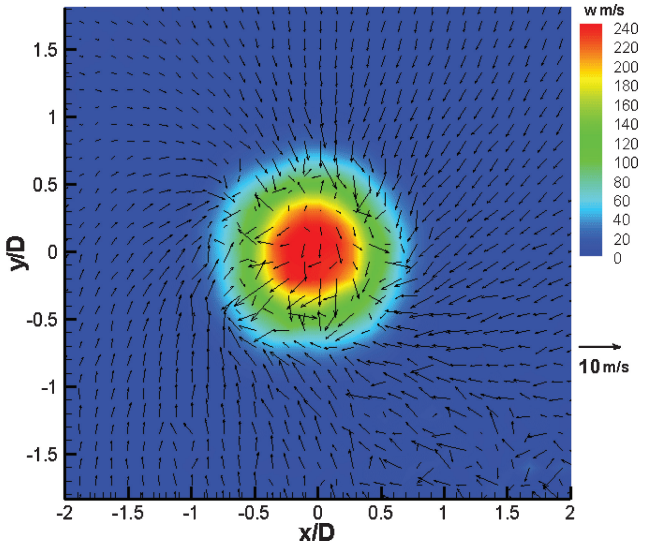

Fig. 10 Stereo DPIV ensemble-averaged velocity map at $z/D = 4.3$. The w component of velocity is represented by the color contours, and the in-plane u, v components are represented by the velocity vectors.

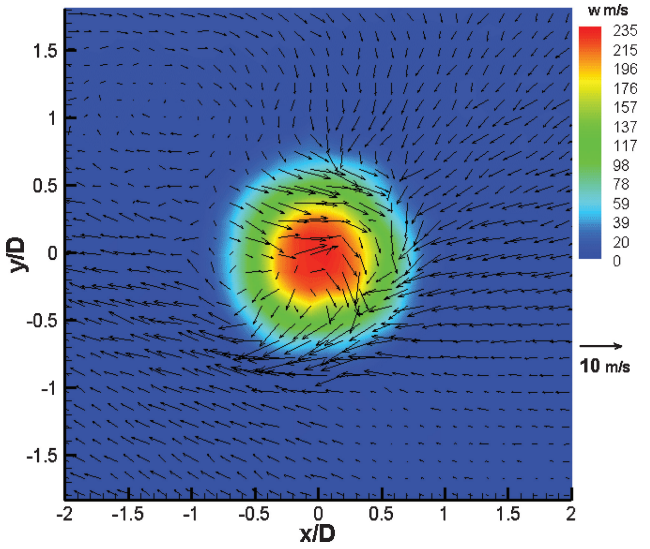

Fig. 11 PPIDV ensemble-averaged velocity map at $z/D = 4.3$. The w component of velocity is represented by the color contours, and the in-plane u, v components are represented by the velocity vectors.

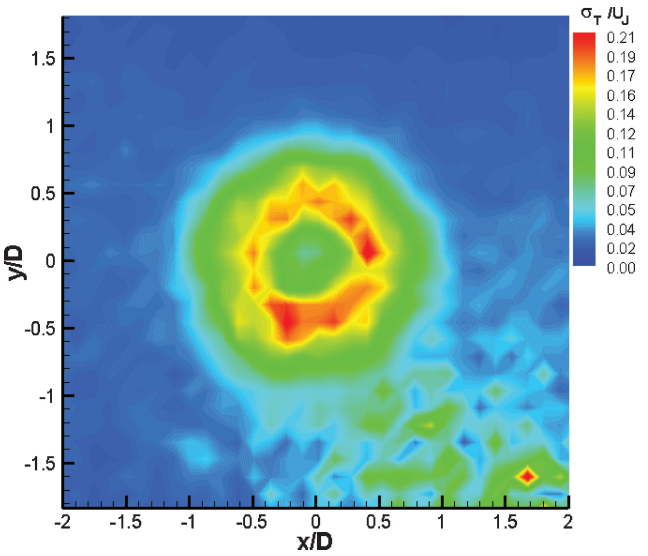

Fig. 12 Stereo DPIV turbulence intensity. The noise in the lower right is from the low seed concentration. The shear layer is clearly evident surrounding the core flow.

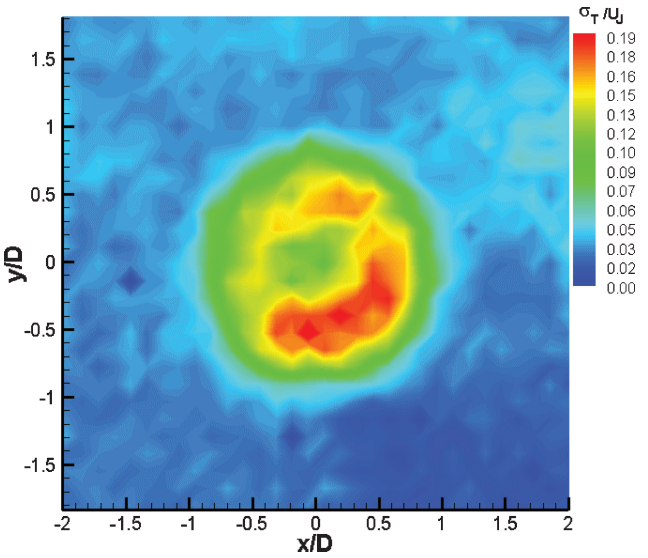

Fig. 13 PPIDV turbulence intensity. The thickness of the shear layer is larger than that obtained with stereo DPIV.

The ensemble-averaged velocity vector map is shown in Fig. 10. The color contours represent the w component of velocity and the in-plane u and v components are shown as vectors. The coordinate axes in the plot are normalized by the jet diameter $D = 9.5$ mm. A reference vector is also shown on the plot. The maximum velocity at the core of the jet is measured to be 245 m/s. The u and v components of velocity are relatively uniform illustrating a slight swirl pattern in the ambient flow. The lack of seed material in the lower right portion of the field of view is manifested in the spurious vectors observed in this region. The vectors in the periphery of the jet core are somewhat randomly oriented, which is probably caused by the turbulent shear layer surrounding the jet flow.

The PPIDV image data were processed according to the steps outlined in the PPIDV Data-Processing Steps section. The frame-straddling image pairs from the signal and reference cameras were processed to obtain the in-plane velocity estimates using standard DPIV correlation processing. A multipass correlation operation was performed, yielding a final grid resolution of 32×32 pixel subregions on 16 pixel centers. The two estimates of the in-plane velocity field were then averaged together. The signal and reference images from the injection-seeded laser pulse were then processed to obtain the Doppler shift estimates of V_m. The high-resolution image data were averaged over 16×16 pixel subregions to match the resolution of the DPIV velocity vector grid, which was 1.2 mm. The in-plane PIV estimates and the estimates of V_m were then used to compute the u, v, and w velocity components. The ensemble-averaged PPIDV velocity data are shown in Fig. 11, where again the w component is represented by the color contours and the in-plane velocity components are denoted by the vectors. The coordinate axes in the plot are normalized by the jet diameter $D = 9.5$ mm. As in the DPIV data processing, the same hard velocity cutoff limits were used along with Chauvenet's criteria for removing statistical outliers. A reference vector is again shown in the plot. The maximum velocity measured at the jet core is 235 m/s. In the PPIDV result, the spatial extent and general shape of the jet core are the same as the DPIV result. The velocity vectors in the ambient flow are slightly less orderly than in the DPIV case. There is significantly less spurious noise in the lower right region of the image than in the DPIV result. The slightly higher degree of randomness in the ambient velocity field in the PPIDV result could be caused by fluctuations in the measured Doppler shift velocity (less accurate at low velocities), which is used to correct the in-plane u-component displacement-based

estimates. The PPIDV result indicates that there is a stronger swirl flow surrounding the nozzle core than in the DPIV result. In both techniques, the error in the estimated velocity outside the jet core is nominally 20%. Therefore it is difficult to determine which result more closely represents the true flowfield.

The sequence of velocity vector maps obtained from each technique was then used to compute the total turbulence $\sigma_T^2 = \sqrt{(\sigma_u^2 + \sigma_v^2 + \sigma_w^2)}$, where σ_u, σ_v, and σ_w are the standard deviations in the measured u, v, and w velocity components. Dividing the total turbulence by the jet efflux velocity U_j yields a map of the turbulence intensity in the flow. Figure 12 shows a color contour map of the turbulence intensity for the DPIV results. The noise in the lower right corner is from the low flow seeding in this region. The turbulence intensity is low in the core of the jet and peaks at the nozzle lip line at approximately 21%. The shear layer is observed around the entire periphery of the jet core. The PPIDV turbulence intensity results are shown in Fig. 13. The turbulence intensity is low at the center of the jet and again increases to approximately 19% at the nozzle lip line. The shear layer is clearly delineated in the right-hand side of the plot and only marginally visible in the left-hand side. This trend is also observed in the DPIV results. The shear layer in the PPIDV result appears to have a larger spatial extent than in the DPIV result. The relatively small sample size (79 vector maps) used to compute these statistics might explain the poor definition and spatial extent of the shear layer.

Uncertainty in the Measurements

Stereo PIV Measurements

The coupling half-angle α in the stereo DPIV system was set to ± 30 deg in order to obtain high accuracy in both the in-plane and out-of-plane measurements. Because the primary flow direction was oriented perpendicular to the plane of the light sheet, the interframe time was kept short (2.47 μs) in order to keep the particles within the plane of the light sheet for both exposures. The relative error in the stereo DPIV measurements is inversely proportional to the displacement between exposures. Here we assume that the error in estimating the correlation peak location can be determined to ± 0.1 pixels, which corresponds to an absolute error of 2.0 m/s. The absolute error in the w component, defined by the coupling angle, is then 3.4 m/s. The maximum x displacements in the nozzle core were on the order of five pixels, yielding a full-scale, single-shot accuracy of 2% in the u component of velocity. The relatively small v velocity resulted in errors of around 20% in the v-component estimates. The u, v, and w relative error levels in the ambient regions were significantly higher as a result of the lower velocities in these regions.

PPIDV Measurements

The rotating wheel measurements showed that the absolute error in measuring the flow velocity using the Doppler shift was 1.6 m/s, which agrees with previously reported results.[2,3,12] As the error analysis showed in Fig. 4, the error in estimating the true w component of velocity was approximately 5.3 m/s for the experimental configuration used here. At the maximum flow velocity to be measured in the nozzle flow of $\approx$232 m/s, the relative error in the w component of velocity is 2.2% at the nozzle centerline, but relatively large in the low velocity ambient flow surrounding the jet. Because the Doppler shift estimates are used to correct the displacement-based velocity estimates, we expect that the low velocity estimates in the periphery of the jet are contaminated by the fixed error in the Doppler shift velocity estimates. The absolute error in the displacement-based velocity estimates was 3 m/s. (This error is higher for the PPIDV results because the field of view was larger for the PPIDV system.) However, averaging the displacement estimate results from the signal and reference cameras reduces this error by $\sqrt{2}$. Hence, the absolute error in the v-component estimates was on the order of 2.1 m/s. The absolute error in the u-component velocity estimates is a combination of the Doppler shift error and the x-component displacement-based error. The PPIDV pan angle of 16 deg resulted in smaller projected in-plane displacements than in the stereo DPIV results. The maximum in-plane x displacement for the PPIDV results was on the order of two pixels. The absolute error in the u-component velocity estimates at a pan angle of 16 deg is obtained from Fig. 4 and found to be on the order of 3 m/s.

Note that for the PPIDV system the errors in the core flow region are dominated by the displacement-based velocity results, not by the Doppler shift measurements. The absolute error in the w component of velocity is lower for the for stereo PIV system than the value estimated for the PPIDV technique. The w-component error for the stereo PIV technique can easily exceed the PPIDV error levels if the coupling angle is decreased over the value used here. The v-component errors are relatively the same for the two techniques. The interaction of the Doppler shift and in-plane x-displacement measurements yields an absolute error in the u component of velocity that is higher than that expected in the stereo PIV system.

Conclusions

A new technique, called planar particle imaging Doppler velocimetry (PPIDV), has been presented, which combines the DPIV and DGV techniques in order to facilitate the acquisition of three-component, planar velocity measurements from a single viewing direction. The data-acquisition and processing strategies for the new technique are presented. An error analysis is presented, which shows that the errors in the PPIDV technique are comparable to those obtained using standard stereo DPIV. This is a significant achievement considering that we have collapsed the measurement requirement to a single viewing direction. Orthogonal viewing of the light-sheet plane provides measurements of u and v that are independent of the Doppler shift measurement. For all pan angles > 0 deg, the displacement-based estimates are contaminated by the out-of-plane velocity component. A procedure was presented for correcting the out-of-plane motion error in the displacement-based estimates, using the Doppler shift estimate of velocity.

Although high-resolution image data were acquired (1280×1024), the Doppler shift data were processed on a spatial resolution comparable to that obtained with PIV, that is, 16×16 pixel subregions. The use of 16-pixel binning in the Doppler shift processing of the image data minimized any speckle noise in the final result.

Measurements of a rotating wheel were used to quantify the systematic error in the Doppler shift measurement portion of the technique. These results indicated that the error in the Doppler shift measurement was on the order of 1.6 m/s. Measurements of a nozzle flow were obtained using an experimental setup, which enabled simultaneous acquisition of stereo DPIV and PPIDV measurements. The ensemble averaged measurement results for the two techniques are very similar. The turbulence fields measured by both techniques were very similar, clearly delineating the shear layer in the nozzle flow. In general, the PPIDV technique is slightly less accurate than the stereo PIV technique. For low-speed flows, the stereo PIV technique will generally be more accurate. However, in high-speed flows both techniques yield flow measurement results of comparable accuracy.

Although the setup, calibration, and data analysis are slightly more involved than stereo DPIV, the new technique appears to be a viable alternative to conventional techniques and especially attractive for limited optical access flows. The equipment requirements are comparable to that of stereo DPIV because a single pair of frame-straddling cameras are required. Although in this work only one of the laser pulses was injection seeded, two injection-seeded lasers could be used in the technique to provide another independent estimate of the w-velocity component. We anticipate that proper operation of the injection seed laser Q switch at 10 Hz and better utilization of the laser beam spatial frequency distribution will yield improved accuracy results in the future.

Acknowledgments

The author thanks Wentworh John, Gary Clayo, and Anthony Opalski for their efforts in the setup and implementation of the PPIDV system. Discussions and assistance from James Meyers from NASA Langley Research Center were invaluable to the successful implementation of the DGV portion of the technique. His assistance is greatly appreciated.

References

[1]Wernet, M. P., "Stereo Viewing 3-Component, Planar PIV Utilizing Fuzzy Inference," AIAA Paper 96-2268, June 1996.

[2]Meyers, J. F., Lee, J. W., and Schwartz, R. J., "Characterization of Measurement Error Sources in Doppler Global Velocimetry," *Measurement Science and Technology*, Vol. 12, 2001, pp. 357–368.

[3]Clancy, P. S., and Samimy, M., "Two-Component Planar Doppler Velocimetry in High-Speed Flows," *AIAA Journal*, Vol. 35, No. 11, 1997, pp. 1729–1738.

[4]Samimy, M., and Wernet, M. P., "Review of Planar Multiple-Component Velocimetry in High-Speed Flows," *AIAA Journal*, Vol. 38, No. 4, 2000, pp. 553–574.

[5]Roehle, I., Willert, C., and Schodl, R., "Recent Applications of Three-Dimensional; Doppler Global Velocimetry in Turbomachinery," *Proceedings of the 9th International Symposium on Applications of Laser Techniques to Fluid Mechanics*, 1998.

[6]Wernet, M. P., "Planar Particle Imaging Doppler Velocimetry System and Method," U.S. Patent 6,542,226 B1, issued 1 April 2003.

[7]Boemmels, R., and Roesgen, T., "Development of a Planar Three Component Velocimeter Using Doppler Global Velocimetry (DGV) and PIV," *Proceedings of the 19th International Congress on Instrumentation for Use in Aerospace Simulation Facilities (ICIASF)*, Cleveland, OH, 2001, pp. 211–218.

[8]Raffel, M., Willert, C., and Kompenhans, J., *Particle Image Velocimetry, a Practical Guide*, Springer-Verlag, Berlin, 1998, pp. 1–12.

[9]Westerweel, J., and Nieuwstadt, F. T. M., "Performance Tests on 3-Dimensional Velocity Measurements with a Two-Camera Digital Particle-Image Velocimeter," *Fourth International Conference on Laser Anemometry*, Vol. 1, edited by A. Dybbs and B. Ghorashi, Cleveland, OH, 1991, pp. 349–355.

[10]Smith, M. W., "The Reduction of Laser Speckle Noise in Planar Doppler Velocimetry Systems," AIAA Paper 98-2607, 1998.

[11]Forkey, J. N., "Development and Demonstration of Filtered Rayleigh Scattering—a Laser Based Flow Diagnostic for Planar Measurements of Velocity, Temperature and Pressure," NASA Graduate Student Researcher Final Report, Grant NGT-50826, 1996.

[12]McKenzie, R. L., "Planar Doppler Velocimetry Performance in Low-Speed Flows," AIAA Paper 97-0498, Jan. 1997.

[13]Bevington, P. R., *Data Reduction and Error Analysis for the Physical Sciences*, McGraw–Hill, New York, 1969, p. 60.

[14]Taylor, J. R., *An Introduction to Error Analysis*, Univ. Science Books, Oxford Univ. Press, Mill Valley, CA, 1982, pp. 141–143.

J. Trolinger
Guest Editor

Color reproductions courtesy of NASA Glenn's Independent Research and Development Program.